Journal of Sound and Vibration (2002) **257**(4), 713–731
doi:10.1006/jsvi.5040, available online at http://www.idealibrary.com on IDEAL®

ANALYSIS OF NON-LINEAR DYNAMIC STABILITY FOR A ROTATING SHAFT-DISK WITH A TRANSVERSE CRACK

Y. M. Fu and Y. F. Zheng

Department of Engineering Mechanics Hunan University, Changsha, Hunan, People's Republic of China. E-mail: yfzheng2000@163.net

AND

Z. K. Hou

Department of Mechanical Engineering, Worcester Polytechnic Institute, Worcester, U.S.A.

(*Received* 10 *September* 2001, *and in final form* 18 *December* 2001)

In this paper, the nonlinear dynamic stability of a rotating shaft-disk with a transverse crack is studied. The crack and the disk are located in arbitrary positions of the shaft respectively. Using the equivalent line-spring model, the deflections of the system with a crack are constructed by adding a deflection to the deflections of the uncracked system. The unstable regions are confirmed by Runge–Kutta method and the Floquet theory. The effects of crack depth, crack position, disk position, disk thickness and rotating speed on the principal unstable regions are discussed. The numerical results are compared with available data.

1. INTRODUCTION

High-speed and light-structure is the design-trend of the modern rotating machines, but it is easy for unstable phenomena to occur, which brings many serious accidents. Therefore, in recent years, the dynamic stability behaviour of the rotor system has received considerable attention. However, very little of the literature is concerned with the mass of the shaft, the additional displacement caused by the crack and the geometric non-linearity of the shaft.

The dynamic instability of a rotating asymmetric shaft with internal viscous damping supported in anisotropic bearings was studied by Wettergren [1] and the results indicated the system was unstable according to Floquet theory. The stability and vibration of a rotating circular plate subjected to stationary in-plane edge loads were investigated by Shen [2] and the boundaries of the unstable regions were confirmed through multiple scales method. By using the transfer matrix method, Guilhen [3] studied the instability and imbalance responses of unsymmetrical rotor-bearing systems. Jia [4] obtained the natural frequencies of a Timoshenko shaft carrying elastic disks. Chung [5] studied the non-linear vibration of a flexible spinning disk with angular acceleration. For the problem of rotor system with crack, Papadopoulos [6–8] discussed the longitudinal and bending coupled vibration of a cantilever beam with a transverse crack. By using a massless spring to replace the stiffness of the location of the cracked shaft and the cosine series to describe the rule of the stiffness which changed during the rotation, he also obtained the local flexibility

0022-460X/02/$35.00

matrix for an open transverse crack and discussed the stability of cracked rotors in the coupled vibration mode. By using a hinge model to explain the stiffness of the cracked shaft, Gasch [9] studied the dynamic behaviour of a simple rotating shaft with a transverse crack. Moreover, [10–12] investigated the dynamic stability and forced vibration of a cracked shaft. Sheu and Chen [13] and Chen and Pen [14] have discussed the dynamic stability of a single rotor under axial parametric exciting. Recently, Sekhar [15] studied the vibration characteristics of a cracked rotor with two open cracks.

All these above studies are found on the rotor system without the mass of the shaft and did not consider the additional displacement caused by the crack. Therefore, these analyses are only proper to a crack located at the mid-span of the shaft, while for the crack located at the other position, the calculated results show bigger error. Moreover, the effect of the geometric non-linearity is not considered in the above systems, but non-linear effects have been recognized to play an important role in determining the stability of the rotor system. In the present investigation, the mass of elastic shaft, the additional displacement caused by the crack and the effect of the geometric non-linearity are taken into account. And the effects of the different parameters on the non-linear dynamic stability of the shaft-disk with a crack are discussed.

2. EQUATIONS OF MOTION

Consider a shaft of radius R_s and length l having a disk of radius R_d at location $\beta_0 = l_0/l$. Assume that the shaft has a crack of depth $h = a/R_s$ at location $\beta_1 = l_1/l$, shown in Figure 1. The cross-section of a circular shaft with a transverse crack is shown in Figure 2.

Also, assume the shaft to be loaded with the axial force P_1, bending moments P_2 in the ζ direction and P_3 in the η direction. The dimension of a local flexibility matrix depends on the number of degrees of freedom considered, here 3×3. According to the theory of fracture mechanics, the release rate of the strain energy for the system is [6, 7]:

$$J = \frac{1 - v^2}{E_s}(K_{I1} + K_{I2} + K_{I3})^2, \tag{1}$$

where v is the Poisson ratio, E_s is Young's modulus of the shaft, K_{I1}, K_{I2} and K_{I3} are the stress intensity factors of the opening mode for the load P_1, P_2 and P_3, respectively, and

$$\begin{aligned} K_{I1} &= \sigma_1\sqrt{\pi\zeta}F_1(\zeta/H), \quad \sigma_1 = P_1/(\pi R_s^2), \\ K_{I2} &= \sigma_2\sqrt{\pi\zeta}F_1(\zeta/H), \quad \sigma_2 = 4P_2\eta/(\pi R_s^4), \\ K_{I3} &= \sigma_3\sqrt{\pi\zeta}F_2(\zeta/H), \quad \sigma_3 = 2P_3H/(\pi R_s^4) \end{aligned} \tag{2}$$

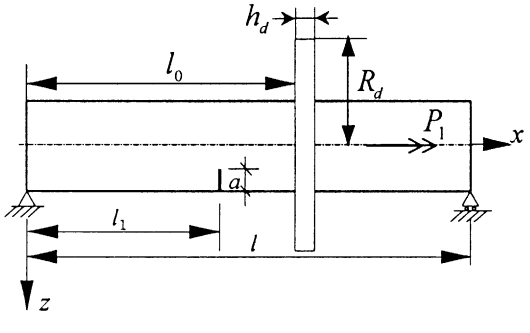

Figure 1. Model of shaft disk with a crack.

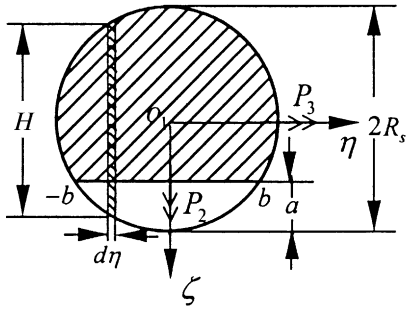

Figure 2. Cross-section of shaft with a crack.

in which

$$\begin{gathered} F_1(\zeta/H) = \sqrt{\tan\lambda/\lambda}\{0{\cdot}752 + 2{\cdot}02(\zeta/H) + 0{\cdot}37[1-\sin\lambda]^3\}/\cos\lambda, \\ F_2(\zeta/H) = \sqrt{\tan\lambda/\lambda}\{0{\cdot}923 + 0{\cdot}199[1-\sin\lambda]^4\}/\cos\lambda, \\ \zeta(\eta) = a - R_s + \sqrt{R_s^2 - \eta^2}, \\ H = 2\sqrt{R_s^2 - \eta^2}, \quad \lambda = \pi\zeta/2H. \end{gathered} \tag{3}$$

The local flexibility of the shaft due to the crack is [6, 7]

$$C_{Lij} = \partial^2 \int_{-b}^{b}\int_{0}^{\zeta} J(\zeta)\,\mathrm{d}\zeta\,\mathrm{d}\eta/\partial P_i \partial P_j \quad (i, j = 1, 2, 3). \tag{4}$$

Substituting equations (1)–(3) into equation (4), the local flexibility matrix occurred by crack is written as

$$[C_{Loc}] = \begin{bmatrix} C_{L11} & C_{L12} & C_{L13} \\ C_{L12} & C_{L22} & C_{L23} \\ C_{L13} & C_{L23} & C_{L33} \end{bmatrix}_{Loc}. \tag{5}$$

Now, the shaft is assumed to rotate with a constant speed Ω, and the crack is assumed to be open at its lower position, and closed at its upper position due to gravity [8, 11]. Hence, the additional flexibility depends on the rotating angle of the shaft and it is denoted by matrix $[C]$. This variation of additional flexibility with time t can be expressed by the truncated cosine series and written as follows:

$$[C] = [C_0] + [C_1]\cos\Omega t + [C_2]\cos 2\Omega t + [C_3]\cos 3\Omega t + [C_4]\cos 4\Omega t, \tag{6}$$

where $[C_i](i = 0, 1, \ldots, 4)$ is a 3×3 matrix and can be determined by the following known conditions:

$$\begin{aligned} [C] &= [C_{Loc}], & \phi &= \Omega t = 0, \\ \partial^2[C]/\partial\phi^2 &= 0, & \phi &= \Omega t = 0, \\ [C] &= [C'_{Loc}], & \phi &= \Omega t = \pi/2, \\ [C] &= 0, & \phi &= \Omega t = \pi, \\ \partial^2[C]/\partial\phi^2 &= 0, & \phi &= \Omega t = \pi. \end{aligned} \tag{7}$$

and in which

$$[C'_{Loc}] = \frac{1}{2}\begin{bmatrix} C_{L11} & C_{L13} & C_{L12} \\ C_{L13} & C_{L33} & C_{L23} \\ C_{L12} & C_{L23} & C_{L22} \end{bmatrix}_{Loc}. \tag{8}$$

The dimensionless form of the local flexibility matrix is

$$[\bar{C}_{Loc}] = \begin{bmatrix} \bar{C}_{L11} & \bar{C}_{L12} & \bar{C}_{L13} \\ \bar{C}_{L12} & \bar{C}_{L22} & \bar{C}_{L23} \\ \bar{C}_{L13} & \bar{C}_{L23} & \bar{C}_{L33} \end{bmatrix}_{Loc}, \tag{9}$$

where:

$$\begin{aligned}
\bar{C}_{L11} &= \pi E_s R_s C_{L11}/(1-\nu^2) = 4\int_0^{\bar{b}}\int_0^{\bar{\zeta}} \bar{\zeta} F_1^2(\bar{H})\,\mathrm{d}\bar{\zeta}\,\mathrm{d}\bar{\eta}, \\
\bar{C}_{L12} &= \pi E_s R_s^2 C_{L12}/(1-\nu^2) = 16\int_0^{\bar{b}}\int_0^{\bar{\zeta}} \bar{\zeta}\bar{\eta} F_1^2(\bar{H})\,\mathrm{d}\bar{\zeta}\,\mathrm{d}\bar{\eta}, \\
\bar{C}_{L13} &= \pi E_s R_s^2 C_{L13}/(1-\nu^2) = 16\int_0^{\bar{b}}\int_0^{\bar{\zeta}} \bar{\zeta}(1-\bar{\eta}^2)^{1/2} F_1(\bar{H}) F_2(\bar{H})\,\mathrm{d}\bar{\zeta}\,\mathrm{d}\bar{\eta}, \\
\bar{C}_{L22} &= \pi E_s R_s^3 C_{L11}/(1-\nu^2) = 64\int_0^{\bar{b}}\int_0^{\bar{\zeta}} \bar{\zeta}\bar{\eta}^2 F_1^2(\bar{H})\,\mathrm{d}\bar{\zeta}\,\mathrm{d}\bar{\eta}, \\
\bar{C}_{L33} &= \pi E_s R_s^3 C_{L22}/(1-\nu^2) = 64\int_0^{\bar{b}}\int_0^{\bar{\zeta}} \bar{\zeta}(1-\bar{\eta}^2) F_2^2(\bar{H})\,\mathrm{d}\bar{\zeta}\,\mathrm{d}\bar{\eta}, \\
\bar{C}_{L23} &= \pi E_s R_s^3 C_{L12}/(1-\nu^2) = 64\int_0^{\bar{b}}\int_0^{\bar{\zeta}} \bar{\zeta}\bar{\eta}(1-\bar{\eta}^2)^{1/2} F_1(\bar{H}) F_2(\bar{H})\,\mathrm{d}\bar{\zeta}\,\mathrm{d}\bar{\eta}, \\
\bar{b} &= b/R_s, \bar{\zeta} = \zeta/R_s, \bar{\eta} = \eta/R_s, \bar{H} = \zeta/H.
\end{aligned} \tag{10}$$

In order to describe the motion of the system and obtain the total kinetic and potential energy of the system, two co-ordinate systems are used. An $oxyz$ frame represents the inertial system, and $\vec{x}$ is the axial direction of the shaft shown in Figure 1. An $o_1\xi\eta\zeta$ frame is the local reference system fixed to the disk and its origin is located at the centre of the disk, and $\vec{\xi}$ is the normal direction of the disk. The ϑ is an included angle by ξ- and x-axis. The projective line of ξ is O_1P_y in the o_1xy plane, and the projective line of ξ is O_1P_z in the o_1xz plane. ϑ_y is an included angle of O_1P_y and x-axis, and ϑ_z is an included angle of O_1P_z and x-axis. The unit vector of the normal direction of the $o_1x\xi$ plane is defined as $\vec{X} = (\vec{x} \times \vec{\xi})/\sin\vartheta$, shown in Figure 3. The rigid body motion of the disk may be described as follows: firstly, the disk rotates an angle ϑ about X-axis. Then, the disk rotates at an angle Ωt about ξ-axis. Because the axial deformation of the shaft is very small compared with the transverse deformation of the shaft, for simplifying the calculation, the axial deformation of the shaft can be neglected. So the whirling transverse displacements of the shaft is represented by (v_{sc}, w_{sc}) in $oxyz$ system. The transverse displacement of the disk is denoted by w_d in the $o_1\xi\eta\zeta$ system.

Now, the energy expressions are divided. Assume that any point P (the position vector is $\vec{r}$) in the disk changes to P' due to the transverse deformation w_d of the disk, and the position vector $\vec{r'}$ and velocity $\dot{\vec{r'}}$ of the point P' in the disk (shown in Figure 4) are,

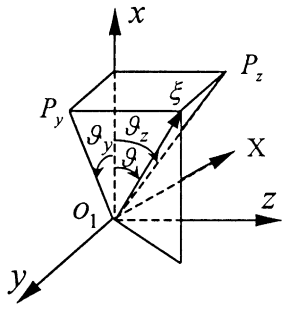

Figure 3. The rigid body motion of the disk.

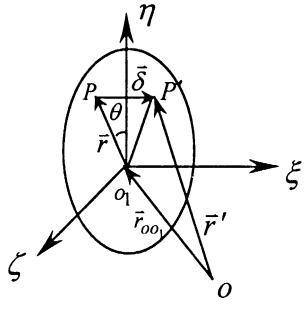

Figure 4. The bending deformation of a disk.

respectively,

$$\vec{r}\,' = \vec{r}_{oo_1} + \vec{r} + \vec{\delta},$$
$$\dot{\vec{r}}\,' = \dot{\vec{r}}_{oo_1} + \vec{\omega} \times \vec{r} + \dot{\vec{\delta}}, \tag{11}$$

where

$$\dot{\vec{r}}_{oo_1} = \left[\frac{\partial v_{sc}}{\partial t} \quad \frac{\partial w_{sc}}{\partial t} \right]_{x=l_0},$$

$$\vec{r} = r\cos\theta\,\vec{\eta} + r\sin\theta\,\vec{\xi}, \quad \vec{\delta} = w_d\,\vec{\xi},$$

$$\vec{\omega} = \left(\frac{\vartheta_z\dot{\vartheta}_y - \vartheta_y\dot{\vartheta}_z}{2} + \Omega \right)\vec{\xi} + (\sin\Omega t\dot{\vartheta}_y - \cos\Omega t\dot{\vartheta}_z)\vec{\eta} + (\cos\Omega t\dot{\vartheta}_y + \sin\Omega t\dot{\vartheta}_z)\vec{\zeta}, \tag{12}$$

$$\vartheta_y = -\left.\frac{\partial w_{sc}}{\partial x}\right|_{x=l_0}, \quad \vartheta_z = \left.\frac{\partial v_{sc}}{\partial x}\right|_{x=l_0}.$$

Therefore, the kinetic energy of the disk is

$$\mathrm{T}_d = \frac{\rho_d h_d}{2}\int_{R_s}^{R_d}\int_0^{2\pi} \dot{\vec{r}}'\,\dot{\vec{r}}'\, r\,\mathrm{d}r\,\mathrm{d}\theta = \frac{1}{2}M_d\left[\left(\frac{\partial v_s}{\partial t}\right)^2 + \left(\frac{\partial w_s}{\partial t}\right)^2\right]_{x=l_0} + \frac{1}{2}J_d(\omega_\eta^2 + \omega_\zeta^2)$$
$$+ \frac{1}{2}J_p\omega_\xi^2 + \frac{1}{2}\rho_d h_d\int_0^{2\pi}\int_{R_s}^{R_d}\left\{\left(\frac{\partial w_d}{\partial t}\right)^2 + 2r[\sin\theta\omega_\eta - \cos\theta\omega_\zeta)]\frac{\partial w_d}{\partial t}\right.$$
$$\left. - 2\Omega r[\sin\theta\omega_\zeta + \cos\theta\omega_\eta)w_d\right\} r\,\mathrm{d}r\,\mathrm{d}\theta, \tag{13}$$

where neglecting the effect of the crack on the rotation angle at the joint-point of the disk and the shaft, ρ_d is the mass per unit volume of the disk, h_d is the thickness of the disk, M_d is the total mass of the disk, J_d and J_p are the rotational inertia moments of the disk mass about the diameter and the axis, respectively, and $J_p = 2J_d$ for a symmetric disk.

The strain energy of the disk can be expressed as

$$\Pi_d = \frac{D}{2}\int_{R_s}^{R_d}\int_0^{2\pi}\left\{\left(\frac{\partial^2 w_d}{\partial r^2} + \frac{1}{r}\frac{\partial w_d}{\partial r} + \frac{1}{r^2}\frac{\partial^2 w_d}{\partial\theta^2}\right)^2 - 2(1-v)\frac{\partial^2 w_d}{\partial r^2}\left(\frac{1}{r}\frac{\partial w_d}{\partial r} + \frac{1}{r^2}\frac{\partial^2 w_d}{\partial\theta^2}\right)\right.$$
$$\left. + 2(1-v)\left[\frac{\partial}{\partial r}\left(\frac{1}{r}\frac{\partial w_d}{\partial\theta}\right)\right]^2\right\} r\,\mathrm{d}r\,\mathrm{d}\theta, \tag{14}$$

where $D = E_d h_d^3/12(1-v^2)$ is the bending rigidity of the disk, E_d is Young's modulus.

Considering the geometric non-linearity, the axial strain ε_{sx} and the curvatures κ_{sy} and κ_{sz} of the flexible curves are given by

$$\varepsilon_{sx} = \frac{1}{2}\left(\frac{\partial v_{sc}}{\partial x}\right)^2 + \frac{1}{2}\left(\frac{\partial w_{sc}}{\partial x}\right)^2, \quad \kappa_{sy} = -\frac{\partial^2 v_{sc}}{\partial x^2}, \quad \kappa_{sz} = -\frac{\partial^2 w_{sc}}{\partial x^2} \tag{15}$$

and the axial internal forces N_s and the internal moments M_{sy} and M_{sz} are

$$N_s = \frac{1}{2}E_s A_s\left[\left(\frac{\partial v_{sc}}{\partial x}\right)^2 + \left(\frac{\partial w_{sc}}{\partial x}\right)^2\right], \quad M_{sy} = -E_s I_s\frac{\partial^2 v_{sc}}{\partial x^2}, \quad M_{sz} = -E_s I_s\frac{\partial^2 w_{sc}}{\partial x^2}, \tag{16}$$

where A_s is the area of the cross-section; and I_s is the axial inertia moment of cross-section of the shaft.

In this case, the strain energy of the shaft may be expressed as

$$\Pi_s = \frac{1}{2}\int_0^l (\varepsilon_{sx}N_s + \kappa_{sy}M_{sy} + \kappa_{sz}M_{sz})\,\mathrm{d}x$$
$$= \frac{1}{2}\int_0^l\left\{E_s A_s\left[\frac{1}{2}\left(\frac{\partial v_{sc}}{\partial x}\right)^2 + \frac{1}{2}\left(\frac{\partial w_{sc}}{\partial x}\right)^2\right]^2 + E_s I_s\left[\left(\frac{\partial^2 v_{sc}}{\partial x^2}\right)^2 + \left(\frac{\partial^2 w_{sc}}{\partial x^2}\right)^2\right\}\mathrm{d}x. \tag{17}$$

The kinetic energy of the shaft is written as

$$\mathrm{T}_s = \frac{1}{2}\int_0^l \rho_s A_s\left[\left(\frac{\partial v_{sc}}{\partial t}\right)^2 + \left(\frac{\partial w_{sc}}{\partial t}\right)^2\right]\mathrm{d}x, \tag{18}$$

where ρ_s is the mass density of the shaft.

The crack-released energy is obtained as

$$\Pi_k = \frac{1}{2}\left[-E_s I_s \frac{\partial^2 v_{sc}}{\partial x^2} \quad -E_s I_s \frac{\partial^2 w_{sc}}{\partial x^2} \right]_{x=l_1} \begin{bmatrix} C_{22} & C_{23} \\ C_{23} & C_{33} \end{bmatrix} \begin{bmatrix} -E_s I_s \dfrac{\partial^2 v_{sc}}{\partial x^2} \\ -E_s I_s \dfrac{\partial^2 w_{sc}}{\partial x^2} \end{bmatrix}_{x=l_1}. \tag{19}$$

As an approximate method, it is possible to divide the entire shaft into two sub-shafts connected by massless springs representing the crack, and to introduce the connecting conditions between the two sub-shafts which ensure the continuity of transverse displacement, bending moment and shear. The continue conditions are written, respectively, as follows:

$$\begin{gathered} v_{sc}|_{x=l_1^+} = v_{sc}|_{x=l_1^-}, \quad w_{sc}|_{x=l_1^+} = w_{sc}|_{x=l_1^-}, \\ \left.\frac{\partial^2 v_{sc}}{\partial x^2}\right|_{x=l_1^+} = \left.\frac{\partial^2 v_{sc}}{\partial x^2}\right|_{x=l_1^-}, \quad \left.\frac{\partial^2 w_{sc}}{\partial x^2}\right|_{x=l_1^+} = \left.\frac{\partial^2 w_{sc}}{\partial x^2}\right|_{x=l_1^-}, \\ \left.\frac{\partial^3 v_{sc}}{\partial x^3}\right|_{x=l_1^+} = \left.\frac{\partial^3 v_{sc}}{\partial x^3}\right|_{x=l_1^-}, \quad \left.\frac{\partial^3 w_{sc}}{\partial x^3}\right|_{x=l_1^+} = \left.\frac{\partial^3 w_{sc}}{\partial x^3}\right|_{x=l_1^-}. \end{gathered} \tag{20}$$

Moreover, the following conditions of equilibrium between bending moment and rotation of the spring are needed at the cracked section due to the slope discontinuity:

$$\begin{aligned} \left.\frac{\partial^2 v_{sc}}{\partial x^2}\right|_{x=l_1^+} - \left.\frac{\partial^2 v_{sc}}{\partial x^2}\right|_{x=l_1^-} &= C_{22} E_s I_s \left.\frac{\partial^2 v_{sc}}{\partial x^2}\right|_{x=l_1}, \\ \left.\frac{\partial^2 w_{sc}}{\partial x^2}\right|_{x=l_1^+} - \left.\frac{\partial^2 w_{sc}}{\partial x^2}\right|_{x=l_1^-} &= C_{33} E_s I_s \left.\frac{\partial^2 w_{sc}}{\partial x^2}\right|_{x=l_1}. \end{aligned} \tag{21}$$

Since the crack is theoretically of zero thickness, the transverse deflection of the cracked shaft consists of the deflection of the shaft without crack and the additional deflection [16]. Then the deflections of the cracked shaft are given as

$$v_{sc} = \begin{cases} v_s - (1-\beta_1) x C_{22} E_s I_s \left.\dfrac{\partial^2 v_s}{\partial x^2}\right|_{x=l_1}, & 0 \leqslant x \leqslant l_1, \\ v_s - \beta_1 (l-x) C_{22} E_s I_s \left.\dfrac{\partial^2 v_s}{\partial x^2}\right|_{x=l_1}, & l_1 \leqslant x \leqslant l, \end{cases} \tag{22a}$$

$$w_{sc} = \begin{cases} w_s - (1-\beta_1) x C_{33} E_s I_s \left.\dfrac{\partial^2 w_s}{\partial x^2}\right|_{x=l_1}, & 0 \leqslant x \leqslant l_1, \\ w_s - \beta_1 (l-x) C_{33} E_s I_s \left.\dfrac{\partial^2 w_s}{\partial x^2}\right|_{x=l_1}, & l_1 \leqslant x \leqslant l. \end{cases} \tag{22b}$$

As an approximate treatment, the displacements of the shaft and the disk substructures will be assumed in a series form of a linear combination of the weighted admissible functions. Due to the fact that only one-nodal diameter modes of the disk couple with the shaft bending modes [4], the transverse displacement of the disk can be written as

$$w_d(r, \theta, t) = W_d(r)[T_{d1}^*(t)\cos\theta + T_{d2}^*(t)\sin\theta], \tag{23}$$

where $W_d(r)$ is the row vector consisting of the admissible functions of the disk, $T_{d1}^*(t)$ and $T_{d2}^*(t)$ are the column vectors consisting of the corresponding time-dependent generalized co-ordinates of the disk.

Here, assume that the spinning disk is clamped at the inner radius $r = R_s$, and is free at the outer radius $r = R_d$. Then, the inner-clamped boundary conditions are

$$w_d|_{r=R_s} = 0, \quad w_d|_{r=R_d} = 0 \tag{24a}$$

and the outer-free boundary conditions are

$$\begin{gathered}\left[\frac{\partial^2 w_d}{\partial r^2} + v\left(\frac{\partial w_d}{r\partial r} + \frac{\partial^2 w_d}{r^2 \partial\theta^2}\right)\right]_{r=R_d} = 0, \\ \left[\frac{\partial}{\partial r}\nabla^2 w_d + \frac{(1-v)\,\partial^2}{r^2 \quad \partial\theta^2}\left(\frac{\partial w_d}{\partial r} - \frac{w_d}{r}\right)\right]_{r=R_d} = 0.\end{gathered} \tag{24b}$$

The shaft bending displacements are expressed as

$$v_s(x,t) = V_s(x)T_v(t), \quad w_s(x,t) = W_s(x)T_w(t), \tag{25}$$

where $V_s(x)$ and $W_s(x)$ are the row vector consisting of the admissible functions of the shaft, and $T_v(t)$ and $T_w(t)$ are the column vectors consisting of the corresponding time-dependent generalized co-ordinates.

Here, assume that the shaft is simply supported at the two ends. So, the ith natural modes for the shaft is given as

$$V_{si}(x) = l\sin\frac{i\pi x}{l}, \quad W_{si}(x) = l\sin\frac{i\pi x}{l}, \quad (i = 1, 2, \ldots, n). \tag{26}$$

The ith natural mode of the disk is defined by

$$W_{di}(r) = (r - R_s)^{i+2}(a_i + b_i r + c_i r^2), \quad (i = 1, 2, \ldots, n). \tag{27}$$

Substituting equations (27) into equations (24b), the boundary conditions may be rewritten as

$$\begin{gathered}\frac{\mathrm{d}^2 W_{di}}{\mathrm{d}r^2} + v\left(\frac{\mathrm{d}W_{di}}{r\,\mathrm{d}r} - \frac{W_{di}}{r^2}\right) = 0, \quad r = R_d \\ \frac{\mathrm{d}(\nabla^2 W_{di})}{\mathrm{d}r} - (1-v)\frac{1}{r^2}\left(\frac{\mathrm{d}W_{di}}{\mathrm{d}r} - \frac{W_{di}}{r}\right) = 0, \quad r = R_d \quad (i = 1, 2, \ldots, n),\end{gathered} \tag{28}$$

where

$$\nabla^2 = \frac{\mathrm{d}^2}{\mathrm{d}r^2} + \frac{\mathrm{d}}{r\,\mathrm{d}r} - \frac{1}{r^2}.$$

The a_i, b_i, c_i are determined from the boundary conditions given by equations (28) and the normalizing conditions are given by

$$W_{di}(R_d) = 1 \quad (i = 1, 2, \ldots, n). \tag{29}$$

For simplified calculation, the first order modes of expressions (23) and (25) are substituted into equations (13), (14) and (17–19). Let $T = T_s + T_d^*$, $\Pi = \Pi_s + \Pi_d + \Pi_k$ and they represent the total kinetic energy and potential energy, respectively, where the detailed expressions are presented in Appendix A. Now, the Lagrange equations are employed and can be written as

$$\frac{d}{dt}\frac{\partial T}{\partial \dot{q}_j} - \frac{\partial T}{\partial q_j} + \frac{\partial \Pi}{\partial q_j} = 0 \quad (j = 1, 2, 3, 4). \tag{30}$$

Substituting the expressions of T and Π into equation (30), and noting that the generalized co-ordinates q_j $(i = 1, 2, 3, 4)$ is T_v, T_w, T_{d1}^* and T_{d2}^*, then, introducing the following

dimensionless parameters:

$$\bar{V}_s(\bar{x}) = V_s(x)/l; \quad \bar{W}_s(\bar{x}) = W_s(x)/l; \quad \bar{W}_d(\bar{r}) = W_d(r)/R_d; \quad \bar{x} = x/l;$$
$$\bar{r} = r/R_d; \quad \tau = \omega_{c1}t, \bar{\Omega} = \Omega/\omega_{c1}; \quad \gamma_1 = R_s/l, \gamma_2 = R_d/R_s; \quad \gamma_3 = h_d/R_d$$
$$\gamma_4 = \rho_d/\rho_s, \gamma_5 = E_d/E_s \tag{31}$$

where ω_{c1} is the first fundamental vibration frequency of the shaft without crack. The dimensionless equations of motion of the system are obtained and can be written as

$$\begin{aligned}
&[\varphi_9 + \varphi_5 - 2\varphi_1\bar{C}_{22} + \varphi_2\bar{C}_{22}^2]\ddot{T}_v - \varphi_{14}\ddot{T}_{d1}^* + [-2\varphi_1\dot{\bar{C}}_{22} + 2\varphi_2\bar{C}_{22}\dot{\bar{C}}_{22}]\dot{T}_v - 2\bar{\Omega}\varphi_{14}\dot{T}_{d2}^* + \bar{\Omega}\varphi_{17}\dot{T}_w \\
&\quad + [-\varphi_1\ddot{\bar{C}}_{22} + \varphi_2\bar{C}_{22}\ddot{\bar{C}}_{22} - \varphi_{11}\bar{C}_{22} + \varphi_7]T_v - \varphi_{12}\bar{C}_{23}T_w + [\varphi_{18} + \varphi_{19}\bar{C}_{22} + \varphi_{20}\bar{C}_{33} \\
&\quad + \varphi_{21}\bar{C}_{22}\bar{C}_{33} + \varphi_{22}\bar{C}_{22}^2 + \varphi_{23}\bar{C}_{33}^2 + \varphi_{24}\bar{C}_{22}\bar{C}_{33}^2 + \varphi_{25}\bar{C}_{22}^2\bar{C}_{33} + \varphi_{26}\bar{C}_{22}^2\bar{C}_{33}^2]T_vT_w^2 \\
&\quad + [\varphi_{27} - \varphi_{28}\bar{C}_{22} + \varphi_{29}\bar{C}_{22}^2 - \varphi_{30}\bar{C}_{22}^3 + \varphi_{31}\bar{C}_{22}^4]T_v^3 = 0,
\end{aligned} \tag{32a}$$

$$\begin{aligned}
&[\varphi_{10} + \varphi_6 - 2\varphi_3\bar{C}_{33} + \varphi_4\bar{C}_{33}^2]\ddot{T}_w - \varphi_{15}\ddot{T}_{d2}^* + [-2\varphi_3\dot{\bar{C}}_{33} + 2\varphi_4\bar{C}_{33}\dot{\bar{C}}_{33}]\dot{T}_w + 2\bar{\Omega}\varphi_{15}\dot{T}_{d1}^* - \bar{\Omega}\varphi_{17}\dot{T}_v \\
&\quad + [-\varphi_3\ddot{\bar{C}}_{33} + \varphi_4\bar{C}_{33}\ddot{\bar{C}}_{33} - \varphi_{13}\bar{C}_{33} + \varphi_8]T_w - \varphi_{12}\bar{C}_{23}T_v + [\varphi_{18} + \varphi_{19}\bar{C}_{22} + \varphi_{20}\bar{C}_{33} \\
&\quad + \varphi_{21}\bar{C}_{22}\bar{C}_{33} + \varphi_{22}\bar{C}_{22}^2 + \varphi_{23}\bar{C}_{33}^2 + \varphi_{24}\bar{C}_{22}\bar{C}_{33}^2 + \varphi_{25}\bar{C}_{22}^2\bar{C}_{33} + \varphi_{26}\bar{C}_{22}^2\bar{C}_{33}^2]T_v^2T_w \\
&\quad + [\varphi_{32} - \varphi_{33}\bar{C}_{33} + \varphi_{34}\bar{C}_{33}^2 - \varphi_{35}\bar{C}_{33}^3 + \varphi_{36}\bar{C}_{33}^4]T_w^3 = 0,
\end{aligned} \tag{32b}$$

$$\ddot{T}_{d1}^* - \frac{\varphi_{14}}{\varphi_{16}}\ddot{T}_v - 2\bar{\Omega}\frac{\varphi_{15}}{\varphi_{16}}\dot{T}_w + 2\bar{\Omega}\dot{T}_{d2}^* + (\alpha^2 - \bar{\Omega}^2)T_{d1}^* = 0, \tag{32c}$$

$$\ddot{T}_{d2}^* - \frac{\varphi_{15}}{\varphi_{16}}\ddot{T}_w + 2\bar{\Omega}\frac{\varphi_{14}}{\varphi_{16}}\dot{T}_v - 2\bar{\Omega}\dot{T}_{d1}^* + (\alpha^2 - \bar{\Omega}^2)T_{d2}^* = 0. \tag{32d}$$

Note that the superscript (.) denotes differentiation with respect to time τ, and the terms α^2 and $\varphi_i (i = 1, \ldots, 36)$ are given in Appendix B.

3. SOLUTION METHODOLOGY

Firstly, consider the linear dynamic stability of the system. Omitting the non-linear terms in equations (32), the linear equations with time-dependent coefficients are obtained. According to the theory of linear differential equations with periodic coefficients, the boundaries between stable and unstable regions can be constructed by periodic solutions with period T and $2T$ in which $T = 2\pi/\bar{\Omega}$. So, the solutions with period $2T$ in terms of τ can be taken in the form of

$$\begin{aligned}
T_w(\tau) &= \sum_{k=1,\,3,\,5,\,\ldots}^{\infty}\left(a_{wk}\cos\frac{k\bar{\Omega}\tau}{2} + b_{wk}\sin\frac{k\bar{\Omega}\tau}{2}\right), \\
T_v(\tau) &= \sum_{k=1,\,3,\,5,\,\ldots}^{\infty}\left(a_{vk}\cos\frac{k\bar{\Omega}\tau}{2} + b_{vk}\sin\frac{k\bar{\Omega}\tau}{2}\right), \\
T_{d1}^*(\tau) &= \sum_{k=1,\,3,\,5,\,\ldots}^{\infty}\left(a_{d1k}\cos\frac{k\bar{\Omega}\tau}{2} + b_{d1k}\sin\frac{k\bar{\Omega}\tau}{2}\right), \\
T_{d2}^*(\tau) &= \sum_{k=1,\,3,\,5,\,\ldots}^{\infty}\left(a_{d2k}\cos\frac{k\bar{\Omega}\tau}{2} + b_{d2k}\sin\frac{k\bar{\Omega}\tau}{2}\right).
\end{aligned} \tag{33a}$$

The solutions with period T in terms of τ can be taken in the form of

$$T_w(\tau) = b_{w0} + \sum_{k=2,4,6,\ldots}^{\infty} \left(a_{wk} \cos \frac{k\bar{\Omega}\tau}{2} + b_{wk} \sin \frac{k\bar{\Omega}\tau}{2} \right),$$

$$T_v(\tau) = b_{v0} + \sum_{k=2,4,6,\ldots}^{\infty} \left(a_{vk} \cos \frac{k\bar{\Omega}\tau}{2} + b_{vk} \sin \frac{k\bar{\Omega}\tau}{2} \right),$$

$$T_{d1}^{*}(\tau) = b_{d10} + \sum_{k=2,4,6,\ldots}^{\infty} \left(a_{d1k} \cos \frac{k\bar{\Omega}\tau}{2} + b_{d1k} \sin \frac{k\bar{\Omega}\tau}{2} \right),$$

$$T_{d2}^{*}(\tau) = b_{d20} + \sum_{k=2,4,6,\ldots}^{\infty} \left(a_{d2k} \cos \frac{k\bar{\Omega}\tau}{2} + b_{d2k} \sin \frac{k\bar{\Omega}\tau}{2} \right). \tag{33b}$$

substituting series (33a) or (33b) into the linear differential equations deriving from equations (32), and equating the coefficients of the $\sin k\bar{\Omega}\tau/2$ and the $\cos k\bar{\Omega}\tau/2$ terms, a set of linear homogeneous algebraic equations with the unknown coefficients a_{wk}, b_{wk}, ..., b_{d2k} can be obtained. The condition for the set of linear equations to have non-trivial solutions is the coefficient determinant of the equations equal to zero. From those, the critical frequencies and the coefficients are determined, and the boundaries of the dynamic unstable regions can be obtained.

In order to validate that analysis is reasonable in this paper, the obtained results are compared with available results shown in Figure 5. The principal dynamic unstable regions are indicated by the areas between the two curves and the solid line denotes the present result, while the point line denotes the result in reference [11]. It is shown that the results approximately agree with each other, but there is also a little difference, because the displacement of the cracked shaft is chosen as that of the uncracked shaft mode in reference [11], while in this paper, the displacement of the cracked shaft is that of the uncracked shaft adding an additional deflection caused by the crack.

For obtaining a more simplified calculation pattern, the dynamic unstable regions of the linear system for the shaft carrying rigid disk or elastic disk are calculated, compared and shown in Figures 6 and 7, in which the Poisson ratio $v = 0{\cdot}3$ and the principal dynamic unstable regions are indicated by the areas between the two curves. Figures 6 and 7 show that the difference is little between the linear elastic shaft carrying elastic disk and the linear elastic shaft carrying rigid disk for the principal unstable regions. So, the transverse displacement of the disk due to elastic deformation will be neglected in the present analysis.

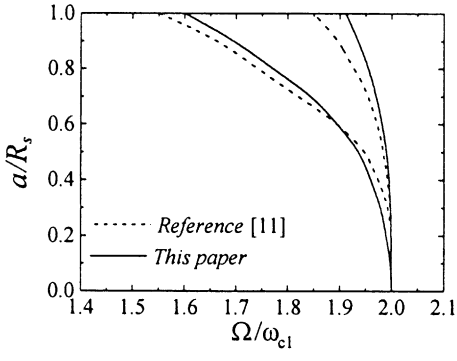

Figure 5. A comparison of the principal dynamic unstable region ($v = 0{\cdot}3$, $\gamma_1 = 0{\cdot}05$, $\gamma_2 = 0$, $\gamma_3 = 0$, $\gamma_4 = 0$, $\gamma_5 = 0$, $\beta_0 = 0$, $\beta_1 = 0{\cdot}5$).

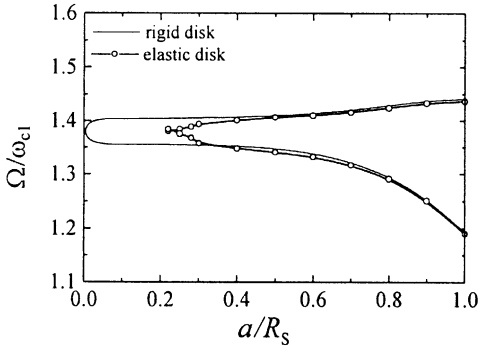

Figure 6. Effect of the flexibility of the disk on the linear principal dynamic unstable regions ($\gamma_1 = 0{\cdot}05$, $\gamma_2 = 5$, $\gamma_3 = 0{\cdot}1$, $\gamma_4 = 1$, $\gamma_5 = 1$, $\beta_0 = 0{\cdot}6$, $\beta_1 = 0{\cdot}4$).

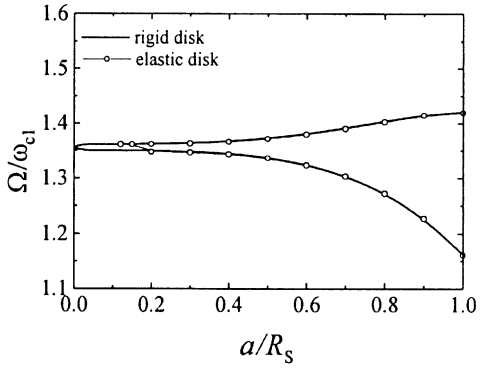

Figure 7. Effect of the flexibility of the disk on the linear principal dynamic unstable regions ($\gamma_1 = 0{\cdot}05$, $\gamma_2 = 5$, $\gamma_3 = 0{\cdot}1$, $\gamma_4 = 1$, $\gamma_5 = 1$, $\beta_0 = 0{\cdot}5$, $\beta_1 = 0{\cdot}5$).

Then, consider the nonlinear dynamic stability of the system. According to the above analysis and for simplifying the non-linear equations of motion (32), the elastic deformation of the disk can be neglected and the simplified non-linear equations of motion of the system can be written as

$$\dot{\boldsymbol{q}}(\tau) = A(\tau)q(\tau) + f(q(\tau), \tau), \tag{34}$$

where $q(\tau) = (T_v,\ \dot{T}_v,\ T_w,\ \dot{T}_w)^{\mathrm{T}}$, $A(\tau) = A(\tau + T)$ is the coefficient matrix and $f(q(\tau), \tau)$ is the non-linear terms. According to the Floquet theory on the stability of the non-linear differential equations, the motion of the system is stable even though exiting the high order differential term in the system, if the real part of the eigenexponent of the system is negative for all periodic motions. So that, $q(0)$ is chosen to be the unit matrix and $q(\tau)$ is formed by using Runge–Kutta method in the numerical calculations. There exists a non-singular constant matrix Φ which satisfies $q(\tau + T) = \Phi q(\tau)$. When $\tau = 0$ and $q(0) = I$, this leads to $\Phi = q(T)$. Therefore, the state transition matrix Φ can be produced by integrating equation (18) numerically that is done four times, and a solution $q^{(i)}(\tau)$ $(i = 1, \ldots, 4)$ is obtained in each time corresponding to a column matrix of initial conditions. In column matrix, all its elements are equal to zero except the element in the ith row, which is equal to 1. Finally, the Φ is determined by evaluating the $q(\tau)$ when letting $\tau = T$.

From the Floquet theory, the stability criteria of the system are identified by the eigenvalues λ of the following eigenequation:

$$Det[\lambda I - \Phi] = 0.$$

And the stability criteria are briefly described as follow [17]: the system is asymptotically stable when $|\lambda_i| < 1 (i = 1, \ldots, 4)$; the system is stable when $|\lambda_i| \leqslant 1 (i = 1, \ldots, 4)$ and at least one of them equals to 1 with its algebraic multiplicity n being equal to the geometric multiplicity m; the system is unstable when at least one of $|\lambda_i| (i = 1, \ldots, 4)$ is greater than 1, or at least one of $|\lambda_i| (i = 1, \ldots, 4)$ is equal to 1 whose $m < n$.

4. NUMERICAL RESULTS AND DISCUSSION

Several examples for the linear or non-linear principal dynamic unstable regions of rotating shaft-disk with the transverse crack are presented . In all cases, the Poisson ratio $v = 0{\cdot}3$, $\gamma_5 = 1$ and the principal unstable regions are indicated by the areas between two curves.

In Figures 8 and 9, the effects of the thickness of the disk on the principal linear or non-linear dynamic unstable regions of the elastic rotating shaft-disk with a crack are shown,

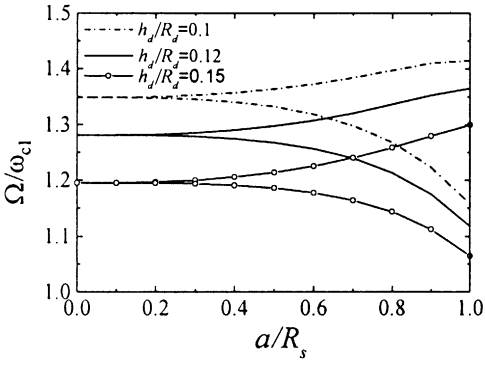

Figure 8. Effect of the thickness of the disk on the linear principal dynamic unstable regions ($\gamma_1 = 0{\cdot}05$, $\gamma_2 = 5$, $\gamma_4 = 1$, $\beta_0 = 0{\cdot}5$, $\beta_1 = 0{\cdot}5$).

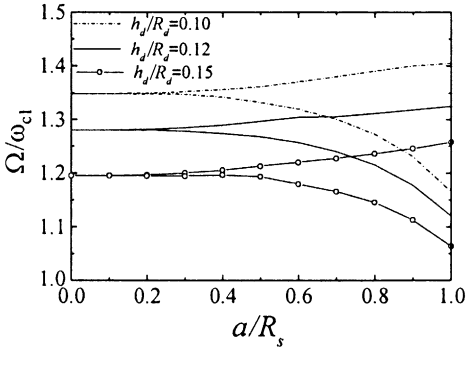

Figure 9. Effect of the thickness of the disk on the non-linear principal dynamic unstable regions ($\gamma_1 = 0{\cdot}05$, $\gamma_2 = 5$, $\gamma_4 = 1$, $\beta_0 = 0{\cdot}5$, $\beta_1 = 0{\cdot}5$).

respectively. It is noted that the thickness of the disk has a pronounced effect on the dynamic stability of elastic shaft–disk rotary system. Following the increasing of the thickness of the disk, the boundaries of the unstable regions are shifted downward, therefore the critical speed of the system is decreased, while the areas of these unstable regions are slightly decreased. Consequently, when designing the rotor system, the disk can be designed as a slight structure to increase the critical speed. Meanwhile, by comparing with the results in the figures, it can be concluded that the geometric non-linearity of the system has certain influence on the dynamic stability of the system and it made the unstable regions become narrower.

From Figures 10 and 11, the effects of the position of the disk on the linear or non-linear principal dynamic unstable regions of the elastic rotating shaft-disk with a crack are given respectively. It can be seen that adjusting the position of the disk can reform the properties of the dynamic stability. Numerical calculations indicate that when the position of the crack is $\beta_1 = 0{\cdot}4$, the critical speed of the system is increased by moving the disk to the right, meanwhile, it makes the unstable region of the system vanish when the crack is little. But the areas of the unstable regions of the whole system become bigger.

The effects of the position of the crack on the linear or non-linear principal dynamic instability regions of the elastic rotating shaft-disk with a crack, respectively, are shown in Figures 12 and 13. It is observed when the position of the crack is in the mid-span of the shaft, the system has the largest dynamic unstable region. The critical speed increases with the increasing of the distance of the crack to the mid-span of the shaft, meanwhile, the

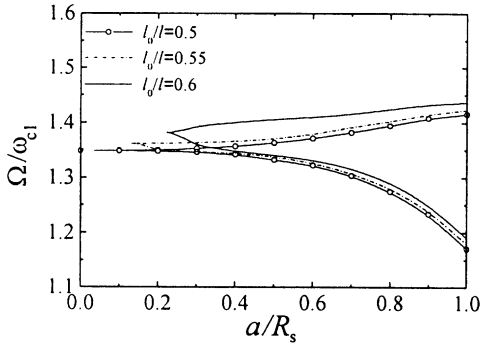

Figure 10. Effect of the location of the disk on the linear principal dynamic unstable regions ($\gamma_1 = 0{\cdot}05$, $\gamma_2 = 5$, $\gamma_3 = 0{\cdot}1$, $\gamma_4 = 1$, $\beta_1 = 0{\cdot}4$).

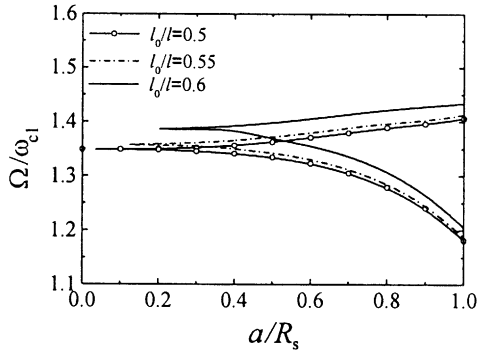

Figure 11. Effect of the location of the disk on the non-linear principal dynamic unstable regions ($\gamma_1 = 0{\cdot}05$, $\gamma_2 = 5$, $\gamma_3 = 0{\cdot}1$, $\gamma_4 = 1$, $\beta_1 = 0{\cdot}4$).

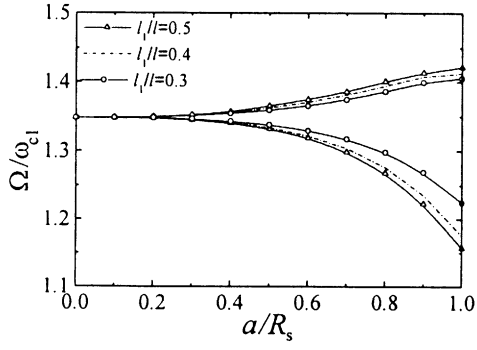

Figure 12. Effect of the location of the crack on the linear principal dynamic unstable regions ($\gamma_1 = 0{\cdot}05$, $\gamma_2 = 5$, $\gamma_3 = 0{\cdot}1$, $\gamma_4 = 1$, $\beta_0 = 0{\cdot}5$).

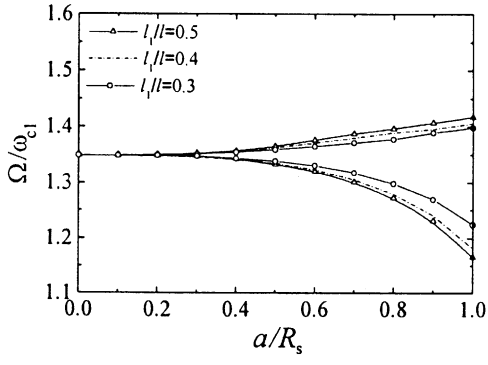

Figure 13. Effect of the location of the crack on the non-linear principal dynamic unstable regions ($\gamma_1 = 0{\cdot}05$, $\gamma_2 = 5$, $\gamma_3 = 0{\cdot}1$, $\gamma_4 = 1$, $\beta_0 = 0{\cdot}5$).

areas of the unstable regions become smaller. By comparing with the results in the figures, it can also be concluded that the geometric non-linearity of the system has certain effect on the dynamic stability of the system and it made the areas of the unstable regions to become smaller.

Also, it can be observed that the depth of the crack has a pronounced influence on the unstable regions and the critical speeds of the system from all the above figures. The areas of the unstable regions become bigger and the critical speeds become lower with increasing the depth of the crack.

5. CONCLUSIONS

The non-linear dynamic stability of a cracked shaft-disk rotor system has been investigated. The principal dynamic unstable regions are confirmed by Floquet theory and Runge–Kutta method. The effects of crack depth, crack position, disk position, disk thickness and rotating speed on the dynamic properties of the system have been discussed. Commonly, the areas of the unstable regions increase and the critical speeds decrease with increasing the depth of the crack. The areas of the unstable regions become smaller and the critical speed increases with increasing the distance of the crack to the mid-span of the shaft. The areas of the unstable regions are slightly decreased and the critical speed is decreased with increasing the thickness of the disk. It can also be concluded that the

geometric non-linearity has certain effect on the dynamic stability of the system and it made the areas of the unstable regions become smaller in all cases. Therefore, for a cracked rotor system, the critical speed and stability of the system can be adjusted by properly selecting the thickness, position of the disk and the crack position, etc.

REFERENCES

1. H. L. Wettergren and K. O. Olsson 1996 *Journal of Sound and Vibration* **195**, 75–84. Dynamic instability of a rotating asymmetric shaft with internal viscous damping supposed in anisotropic bearing.
2. I. Y. Shen and Y. Song 1996 *Journal of Applied Mechanics* **63**, 121–127. Stability and vibration of a rotating circular plate subjected to stationary in-plane edge loads.
3. P. M. Guilhen and P. Berthier 1988 *Journal of Vibration, Acoustics, Stress, and Reliability in Design* **110**, 289–294. Instability and unbalance response of dissymmetric rotor-bearing systems.
4. H. S. Jia 1999 *Journal of Sound and Vibration* **221**, 623–649. On the bending coupled natural frequencies of a spinning, multispan timoshenko shaft carrying elastic disks.
5. J. Chung, J. E. Oh and H. H. Yoo 2000 *Journal of Sound and Vibration* **231**, 375–391. Non-linear vibration of a flexible spinning disc with angular acceleration.
6. C. A. Papadopoulos and A. D. Dimarogonas 1988 *Journal of Vibration, Acoustics, Stress, and Reliability in Design* **110**, 1–8. Coupled longitudinal and bending vibrations of a cracked shaft.
7. C. A. Papadopoulos and A. D. Dimarogonas 1987 *Journal of Sound and Vibration* **117**, 81–93. Coupled longitudinal and bending vibrations of a rotating shaft with an open crack.
8. C. A. Papadopoulos and A. D. Dimarogonas 1988 *Journal of Vibration, Acoustics, Stress, and Reliability in Design* **110**, 356–359. Stability of cracked rotor in the coupled vibration mode.
9. R. Gasch 1993 *Journal of Sound and Vibration* **160**, 313–332. A survey of the dynamic behaviour of a simple rotating shaft with a transverse crack.
10. K. H. Kim and J. H. Kim 2000 *Journal of Sound and Vibration* **233**, 119–135. Effect of a crack on the dynamic stability of a free-free beam subjected to a follower force.
11. S. C. Huang, Y. M. Huang and S. M. Shieh 1993 *Journal of Sound and Vibration* **162**, 387–401. Vibration and stability of a rotating shaft containing a transverse crack.
12 Y. M. Huang and K. K. Chang 1997 *Journal of Sound and Vibration* **202**, 427–437. Stability analysis of a rotating beam under a moving motion-dependent force.
13 Hong-Cheng Sheu and Lien-Wen Chen 2000 *Journal of Sound and Vibration* **234**, 331–348. A lumped mass model for cantilever shaft-disk system.
14. L. W. Chen and W. K. Pen 1998 *Journal of Sound and Vibration* **212**, 215–230. Dynamic stability of rotating composite shaft under periodic axial compressive loads.
15. A. S. Sekhar 1999 *Journal of Sound and Vibration* **223**, 497–512. Vibration characteristics of a cracked rotor with two open cracks.
16. J. Fernandez-Saez, L. Rubic and C. Navarro 1999 *Journal of Sound and Vibration* **225**, 345–352. Approximate calculation of the fundamental frequency for bending vibrations of cracked beams.
17. J. A. Richard 1983 *Analysis of Periodically Time-varying System*. Berlin: Springer-Verlag.

APPENDIX A

The discretized total kinetic energy and potential energy are:
For kinetic energy of disk shaft:

$$T_s = \frac{1}{2}\int_0^l \rho_s A_s \left[\left(\frac{\partial v_{sc}}{\partial t}\right)^2 + \left(\frac{\partial w_{sc}}{\partial t}\right)^2\right] \mathrm{d}x$$

$$= \frac{1}{2}\int_0^{l_1} \rho_s A_s \Big\{ [V_s(x)T_v'(t) - (1-\beta_1)xE_sI_sV_s''(l_1)C_{22}'(t)T_v(t)$$

$$
\begin{aligned}
&- (1-\beta_1)xE_sI_sV_s''(l_1)C_{22}(t)T_v'(t)]^2 \\
&+ W_s(x)T_w'(t) - (1-\beta_1)xE_sI_sW_s''(l_1)C_{33}'(t)T_w(t) \\
&- (1-\beta_1)xE_sI_sW_s''(l_1)C_{33}(t)T_w'(t)]^2\Big\}\,\mathrm{d}x \\
&+\frac{1}{2}\int_{l_1}^{l}\rho_sA_s\Big\{[V_s(x)T_v'(t) - (1-\beta_1)xE_sI_sV_s''(l_1)C_{22}'(t)T_v(t) \\
&- (1-\beta_1)xE_sI_sV_s''(l_1)C_{22}(t)T_v'(t)]^2 \\
&+ [W_s(x)T_w'(t) - (1-\beta_1)xE_sI_sW_s''(l_1)C_{33}'(t)T_w(t) \\
&- (1-\beta_1)xE_sI_sW_s''(l_1)C_{33}(t)T_w'(t)]^2\Big\}\,\mathrm{d}x.
\end{aligned}
$$

For strain energy of the shaft:

$$
\begin{aligned}
\Pi_s =& \frac{1}{8}\Big\{\int_0^{l_1}E_sA_s[V_s'(x) - (1-\beta_1)E_sI_sV_s''(l_1)C_{22}(t)]^4\,\mathrm{d}x \\
&+\int_{l_1}^{l}E_sA_s[V_s'(x) + \beta_1E_sI_sV_s''(l_1)C_{22}(t)]^4\,\mathrm{d}x\Big\}T_v^4(t) \\
&+\frac{1}{4}\Big\{\int_0^{l_1}E_sA_s[V_s'(x) - (1-\beta_1)E_sI_sV_s''(l_1)C_{22}(t)]^2[W_s'(x) \\
&-(1-\beta_1)E_sI_sW_s''(l_1)C_{33}(t)]^2\,\mathrm{d}x \\
&+\int_{l_1}^{l}E_sA_s[V_s'(x) + \beta_1E_sI_sV_s''(l_1)C_{22}(t)]^2[W_s'(x) \\
&+\beta_1E_sI_sW_s''(l_1)C_{33}(t)]^2\,\mathrm{d}x\Big\}T_v^2(t)T_w^2(t) \\
&+\frac{1}{8}\Big\{\int_0^{l_1}E_sA_s[W_s'(x) - (1-\beta_1)E_sI_sW_s''(l_1)C_{33}(t)]^4\,\mathrm{d}x \\
&+\int_{l_1}^{l}E_sA_s[W_s'(x) + \beta_1E_sI_sW_s''(l_1)C_{33}(t)]^4\,\mathrm{d}x\Big\}T_w^4(t) \\
&+\frac{1}{2}\int_0^{l}E_sI_s[V_s''(x)]^2\,\mathrm{d}xT_v^2(t) + \frac{1}{2}\int_0^{l}E_sI_s[W_s''(x)]^2\,\mathrm{d}xT_w^2(t).
\end{aligned}
$$

For kinetic energy of the disk:

$$
\begin{aligned}
T_d =& \frac{1}{2}M_d[V_s^2(l_0)T_v'^2(t) + W_s^2(l_0)T_w'^2(t)] + \frac{1}{2}J_d(\omega_\eta^2 + \omega_\zeta^2 + 2\omega_\xi^2) \\
&- \Omega\begin{bmatrix}\omega_\eta & \omega_\zeta\end{bmatrix}\begin{bmatrix}\Psi_1 & \\ & \Psi_1\end{bmatrix}\begin{bmatrix}T_{d1}\\ T_{d2}\end{bmatrix} \\
&+ \begin{bmatrix}\omega_\eta & \omega_\zeta\end{bmatrix}\begin{bmatrix}& \Psi_1\\ -\Psi_1 & \end{bmatrix}\begin{bmatrix}T_{d1}'\\ T_{d2}'\end{bmatrix} + \frac{1}{2}\begin{bmatrix}T_{d1}' & T_{d2}'\end{bmatrix}\begin{bmatrix}\Psi_2 & \\ & \Psi_2\end{bmatrix}\begin{bmatrix}T_{d1}'\\ T_{d2}'\end{bmatrix},
\end{aligned}
$$

where

$$
\Psi_1 = \rho_d\pi h_d\int_{R_s}^{R_d}r^2W_d(r)\,\mathrm{d}r, \quad \Psi_2 = \rho_d\pi h_d\int_{R_s}^{R_d}rW_d^2(r)\,\mathrm{d}r.
$$

Because ω_η and ω_ζ is the periodic function of time t, in order to eliminating t, we can use the transformation matrix

$$\begin{bmatrix} T_{d1} \\ T_{d2} \end{bmatrix} = \begin{bmatrix} \cos \Omega t & \sin \Omega t \\ -\sin \Omega t & \cos \Omega t \end{bmatrix} \begin{bmatrix} T^*_{d1} \\ T^*_{d2} \end{bmatrix}$$

then, the kinetic energy of the disk can also be written as

$$\begin{aligned} T^*_d = {} & \tfrac{1}{2} M_d [V_s^2(l_0) T_v'^2(t) + W_s^2(l_0) T_w'^2(t)] + \tfrac{1}{2} J_d \{ V_s'^2(l_0) T_v'^2(t) \\ & + W_s'^2(l_0) T_w'^2(t) + 2\Omega [V_s'(l_0) W_s'(l_0) T_v'(t) T_w(t) \\ & - V_s'(l_0) W_s'(l_0) T_v(t) T_w'(t)]\} + 2\Omega \begin{bmatrix} -W_s'(l_0) T_w'(t) & V_s'(l_0) T_v'(t) \end{bmatrix} \begin{bmatrix} & -\Psi_1 \\ \Psi_1 & \end{bmatrix} \begin{bmatrix} T^*_{d1} \\ T^*_{d2} \end{bmatrix} \\ & - \begin{bmatrix} -W_s'(l_0) T_w'(t) & V_s'(l_0) T_v'(t) \end{bmatrix} \begin{bmatrix} \Psi_1 & \\ & \Psi_1 \end{bmatrix} \begin{bmatrix} T'^*_{d1} \\ T'^*_{d2} \end{bmatrix} \\ & + \frac{1}{2} \begin{bmatrix} T'^*_{d1} & T'^*_{d2} \end{bmatrix} \begin{bmatrix} \Psi_2 & \\ & \Psi_2 \end{bmatrix} \begin{bmatrix} T'^*_{d1} \\ T'^*_{d2} \end{bmatrix} \\ & + \Omega \begin{bmatrix} T'^*_{d1} & T'^*_{d2} \end{bmatrix} \begin{bmatrix} & \Psi_2 \\ -\Psi_2 & \end{bmatrix} \begin{bmatrix} T^*_{d1} \\ T^*_{d2} \end{bmatrix} \end{aligned}$$

For strain energy of the disk:

$$\Pi_d = \tfrac{1}{2} K_d T^*_{d1}(t)^2 + \tfrac{1}{2} K_d T^*_{d2}(t)^2$$

in which

$$\begin{aligned} K_d = D\pi \int_{R_s}^{R_d} & \left[W_d''^2(r) + 3 \left[\frac{W_d'(r)}{r} - \frac{W_d(r)}{r^2} \right]^2 \right. \\ & \left. + 2\nu \left[W_d''(r) - \frac{W_d'(r)}{r} + \frac{W_d(r)}{r^2} \right] \cdot \left[\frac{W_d'(r)}{r} - \frac{W_d(r)}{r^2} \right] \right] r \, \mathrm{d}r. \end{aligned}$$

For crack-released energy:

$$\begin{aligned} \Pi_k = {} & \tfrac{1}{2} E_s^2 I_s^2 V_s''^2(l_1) C_{22}(t) T_v^2(t) + E_s^2 I_s^2 V_s''(l_1) W_s''(l_1) C_{23}(t) T_v(t) T_w(t) \\ & + \tfrac{1}{2} E_s^2 I_s^2 W_s''^2(l_1) C_{33}(t) T_w^2(t). \end{aligned}$$

APPENDIX B

The terms α^2 and $\varphi_i (i = 1, \ldots, 36)$ used in equations (32a–32d) are:

$$\alpha^2 = \frac{\gamma_3^2 \gamma_5 \int_{\gamma_2}^1 \left[\bar{W}_d''^2(\bar{r}) + 3 \left(\frac{\bar{W}_d'(\bar{r})}{\bar{r}} - \frac{\bar{W}_d(\bar{r})}{\bar{r}} \right)^2 + 2\nu \left(\bar{W}_d''(\bar{r}) - \frac{\bar{W}_d'(\bar{r})}{\bar{r}} + \frac{\bar{W}_d(\bar{r})}{\bar{r}} \right) \left(\frac{\bar{W}_d'(\bar{r})}{\bar{r}} - \frac{\bar{W}_d(\bar{r})}{\bar{r}} \right) \right] \bar{r} \, \mathrm{d}\bar{r}}{3(1-\nu^2)\pi^4 \gamma_1^4 \gamma_2^2 \gamma_4 \int_{\frac{1}{\gamma_2}}^1 \bar{r} \bar{W}_d^2(\bar{r}) \, \mathrm{d}\bar{r}},$$

$$\varphi_1 = \frac{(1-\nu^2)\gamma_1}{4} \left[\int_0^{\beta_1} (1-\beta_1) \bar{x} \bar{V}_s(\bar{x}) \bar{V}_s''(\beta_1) \, \mathrm{d}\bar{x} + \int_{\beta_1}^1 \beta_1 (1-\bar{x}) \bar{V}_s(\bar{x}) \bar{V}_s''(\beta_1) \, \mathrm{d}\bar{x} \right],$$

$$\varphi_2 = \frac{(1-\nu^2)^2 \gamma_1^2}{16} \left[\int_0^{\beta_1} (1-\beta_1)^2 \bar{x}^2 \bar{V}_s''^2(\beta_1) \, \mathrm{d}\bar{x} + \int_{\beta_1}^1 \beta_1^2 (1-\bar{x})^2 \bar{V}_s''^2(\beta_1) \, \mathrm{d}\bar{x} \right],$$

$$\varphi_3 = \frac{(1-v^2)\gamma_1}{4}\left[\int_0^{\beta_1}(1-\beta_1)\bar{x}\bar{W}_s(\bar{x})\bar{W}_s''(\beta_1)\,\mathrm{d}\bar{x} + \int_{\beta_1}^1 \beta_1(1-\bar{x})\bar{W}_s(\bar{x})\bar{W}_s''(\beta_1)\,\mathrm{d}\bar{x}\right],$$

$$\varphi_4 = \frac{(1-v^2)^2\gamma_1^2}{16}\left[\int_0^{\beta_1}(1-\beta_1)^2\bar{x}^2\bar{W}_s''^2(\beta_1)\,\mathrm{d}\bar{x} + \int_{\beta_1}^1 \beta_1^2(1-\bar{x})^2\bar{W}_s''^2(\beta_1)\,\mathrm{d}\bar{x}\right],$$

$$\varphi_5 = \int_0^1 \bar{V}_s^2(\bar{x})\,\mathrm{d}\bar{x}, \quad \varphi_6 = \int_0^1 \bar{W}_s^2(\bar{x})\,\mathrm{d}\bar{x},$$

$$\varphi_7 = \frac{1}{\pi^4}\int_0^1 \bar{V}_s''^2(\bar{x})\,\mathrm{d}\bar{x}, \quad \varphi_8 = \frac{1}{\pi^4}\int_0^1 \bar{W}_s''^2(\bar{x})\,\mathrm{d}\bar{x},$$

$$\varphi_9 = \gamma_1\gamma_2(\gamma_2^2-1)\gamma_3\gamma_4\bar{V}_s^2(\beta_0) + 0{\cdot}25\gamma_1^3\gamma_2(\gamma_2^4-1)\gamma_3\gamma_4\bar{V}_s'^2(\beta_0),$$

$$\varphi_{10} = \gamma_1\gamma_2(\gamma_2^2-1)\gamma_3\gamma_4\bar{W}_s^2(\beta_0) + 0{\cdot}25\gamma_1^3\gamma_2(\gamma_2^4-1)\gamma_3\gamma_4\bar{W}_s'^2(\beta_0),$$

$$\varphi_{11} = \frac{(1-v^2)\gamma_1}{4\pi^4}\bar{V}_s''^2(\beta_1), \quad \varphi_{12} = \frac{(1-v^2)\gamma_1}{4\pi^4}\bar{V}_s''(\beta_1)\bar{W}_s''(\beta_1),$$

$$\varphi_{13} = \frac{(1-v^2)\gamma_1}{4\pi^4}\bar{W}_s''^2(\beta_1), \quad \varphi_{14} = \gamma_1^3\gamma_2^5\gamma_3\gamma_4\bar{V}_s'(\beta_0)\int_{\frac{1}{\gamma_2}}^1 \bar{r}^2\bar{W}_d(\bar{r})\,\mathrm{d}\bar{r},$$

$$\varphi_{15} = \gamma_1^3\gamma_2^5\gamma_3\gamma_4\bar{W}_s'(\beta_0)\int_{\frac{1}{\gamma_2}}^1 \bar{r}^2\bar{W}_d(\bar{r})\,\mathrm{d}\bar{r}, \quad \varphi_{16} = \gamma_1^3\gamma_2^5\gamma_3\gamma_4\int_{\frac{1}{\gamma_2}}^1 \bar{r}\bar{W}_d^2(\bar{r})\,\mathrm{d}\bar{r},$$

$$\varphi_{17} = 0{\cdot}5\gamma_1^3\gamma_2(\gamma_2^4-1)\gamma_3\gamma_4\bar{V}_s'(\beta_0)\bar{W}_s'(\beta_0),$$

$$\varphi_{18} = \frac{2}{\pi^4\gamma_1^2}\int_0^1 \bar{V}_s'^2(\bar{x})\bar{W}_s'^2(\bar{x})\,\mathrm{d}\bar{x},$$

$$\varphi_{19} = -\frac{1-v^2}{\pi^4\gamma_1}\left[\int_0^{\beta_1}(1-\beta_1)\bar{V}_s'(\bar{x})\bar{W}_s'^2(\bar{x})\bar{V}_s''(\beta_1)\,\mathrm{d}\bar{x} - \int_{\beta_1}^1 \beta_1\bar{V}_s'(\bar{x})\bar{W}_s'^2(\bar{x})\bar{V}_s''(\beta_1)\,\mathrm{d}\bar{x}\right],$$

$$\varphi_{20} = -\frac{1-v^2}{\pi^4\gamma_1}\left[\int_0^{\beta_1}(1-\beta_1)\bar{W}_s'(\bar{x})\bar{V}_s'^2(\bar{x})\bar{W}_s''(\beta_1)\,\mathrm{d}\bar{x} - \int_{\beta_1}^1 \beta_1\bar{W}_s'(\bar{x})\bar{V}_s'^2(\bar{x})\bar{W}_s''(\beta_1)\,\mathrm{d}\bar{x}\right],$$

$$\varphi_{21} = \frac{(1-v^2)^2}{2\pi^4}\left[\int_0^{\beta_1}(1-\beta_1)^2\bar{V}_s'(\bar{x})\bar{W}_s'(\bar{x})\bar{V}_s''(\beta_1)\bar{W}_s''(\beta_1)\,\mathrm{d}\bar{x} + \int_{\beta_1}^1 \beta_1^2\bar{V}_s'(\bar{x})\bar{W}_s'(\bar{x})\bar{V}_s''(\beta_1)\bar{W}_s''(\beta_1)\,\mathrm{d}\bar{x}\right],$$

$$\varphi_{22} = \frac{(1-v^2)^2}{8\pi^4}\left[\int_0^{\beta_1}(1-\beta_1)^2\bar{W}_s'^2(\bar{x})\bar{V}_s''^2(\beta_1)\,\mathrm{d}\bar{x} + \int_{\beta_1}^1 \beta_1^2\bar{W}_s'^2(\bar{x})\bar{V}_s''^2(\beta_1)\,\mathrm{d}\bar{x}\right],$$

$$\varphi_{23} = \frac{(1-v^2)^2}{8\pi^4}\left[\int_0^{\beta_1}(1-\beta_1)^2\bar{V}_s'^2(\bar{x})\bar{W}_s''^2(\beta_1)\,\mathrm{d}\bar{x} + \int_{\beta_1}^1 \beta_1^2\bar{V}_s'^2(\bar{x})\bar{W}_s''^2(\beta_1)\,\mathrm{d}\bar{x}\right],$$

$$\varphi_{24} = -\frac{(1-v^2)^3\gamma_1}{16\pi^4}\left[\int_0^{\beta_1}(1-\beta_1)^3\bar{V}_s'(\bar{x})\bar{V}_s''(\beta_1)\bar{W}_s''^2(\beta_1)\,\mathrm{d}\bar{x} - \int_{\beta_1}^1 \beta_1^3\bar{V}_s'(\bar{x})\bar{V}_s''(\beta_1)\bar{W}_s''^2(\beta_1)\,\mathrm{d}\bar{x}\right],$$

$$\varphi_{25} = -\frac{(1-v^2)^3\gamma_1}{16\pi^4}\left[\int_0^{\beta_1}(1-\beta_1)^3\bar{W}_s'(\bar{x})V_s''^2(\beta_1)\bar{W}_s''(\beta_1)\,\mathrm{d}\bar{x} - \int_{\beta_1}^1 \beta_1^3\bar{W}_s'(\bar{x})\bar{V}_s''^2(\beta_1)\bar{W}_s''(\beta_1)\,\mathrm{d}\bar{x}\right],$$

$$\varphi_{26} = \frac{(1-v^2)^4\gamma_1^2}{128\pi^4}\left[\int_0^{\beta_1}(1-\beta_1)^4\bar{V}_s''^2(\beta_1)\bar{W}_s''^2(\beta_1)\,\mathrm{d}\bar{x} + \int_{\beta_1}^1 \beta_1^4\bar{V}_s''^2(\beta_1)\bar{W}_s''^2(\beta_1)\,\mathrm{d}\bar{x}\right],$$

$$\varphi_{27} = \frac{2}{\pi^4\gamma_1^2}\int_0^1 \bar{V}_s'^4(\bar{x})\,\mathrm{d}\bar{x},$$

$$\varphi_{28} = \frac{2(1-v^2)}{\pi^4\gamma_1}\left[\int_0^{\beta_1}(1-\beta_1)\bar{V}_s'^3(\bar{x})\bar{V}_s''(\beta_1)\,\mathrm{d}\bar{x} - \int_{\beta_1}^1 \beta_1\bar{V}_s'^3(\bar{x})\bar{V}_s''(\beta_1)\,\mathrm{d}\bar{x}\right],$$

$$\varphi_{29} = \frac{3(1-\nu^2)^2}{4\pi^4}\left[\int_0^{\beta_1}(1-\beta_1)^2\bar{V}_s'^2(\bar{x})\bar{V}_s''^2(\beta_1)\,\mathrm{d}\bar{x} + \int_{\beta_1}^1 \beta_1^2\bar{V}_s'^2(\bar{x})\bar{V}_s''^2(\beta_1)\,\mathrm{d}\bar{x}\right],$$

$$\varphi_{30} = \frac{(1-\nu^2)^3\gamma_1}{8\pi^4}\left[\int_0^{\beta_1}(1-\beta_1)^3\bar{V}_s'(\bar{x})\bar{V}_s''^3(\beta_1)\,\mathrm{d}\bar{x} - \int_{\beta_1}^1 \beta_1^3\bar{V}_s'(\bar{x})\bar{V}_s''^3(\beta_1)\mathrm{d}\bar{x}\right],$$

$$\varphi_{31} = \frac{(1-\nu^2)^4\gamma_1^2}{128\pi^4}\left[\int_0^{\beta_1}(1-\beta_1)^4\bar{V}_s''^4(\beta_1)\,\mathrm{d}\bar{x} + \int_{\beta_1}^1 \beta_1^4\bar{V}_s''^4(\beta_1)\,\mathrm{d}\bar{x}\right],$$

$$\varphi_{32} = \frac{2}{\pi^4\gamma_1^2}\int_0^1 \bar{W}_s'^4(\bar{x})\,\mathrm{d}\bar{x},$$

$$\varphi_{33} = \frac{2(1-\nu^2)}{\pi^4\gamma_1}\left[\int_0^{\beta_1}(1-\beta_1)\bar{W}_s'^3(\bar{x})\bar{W}_s''(\beta_1)\,\mathrm{d}\bar{x} - \int_{\beta_1}^1 \beta_1\bar{W}_s'^3(\bar{x})\bar{W}_s''(\beta_1)\,\mathrm{d}\bar{x}\right],$$

$$\varphi_{34} = \frac{3(1-\nu^2)^2}{4\pi^4}\left[\int_0^{\beta_1}(1-\beta_1)^2\bar{W}_s'^2(\bar{x})\bar{W}_s''^2(\beta_1)\,\mathrm{d}\bar{x} + \int_{\beta_1}^1 \beta_1^2\bar{W}_s'^2(\bar{x})\bar{W}_s''^2(\beta_1)\,\mathrm{d}\bar{x}\right],$$

$$\varphi_{35} = \frac{(1-\nu^2)^3\gamma_1}{8\pi^4}\left[\int_0^{\beta_1}(1-\beta_1)^3\bar{W}_s'(\bar{x})\bar{W}_s''^3(\beta_1)\,\mathrm{d}\bar{x} - \int_{\beta_1}^1 \beta_1^3\bar{W}_s'(\bar{x})\bar{W}_s''^3(\beta_1)\,\mathrm{d}\bar{x}\right],$$

$$\varphi_{36} = \frac{(1-\nu^2)^4\gamma_1^2}{128\pi^4}\left[\int_0^{\beta_1}(1-\beta_1)^4\bar{W}_s''^4(\beta_1)\,\mathrm{d}\bar{x} + \int_{\beta_1}^1 \beta_1^4\bar{W}_s''^4(\beta_1)\,\mathrm{d}\bar{x}\right].$$